NASA CONTRACTOR REPORT

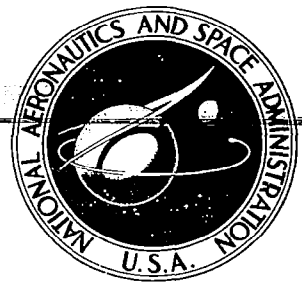

NASA CR-2839

CONSTITUTIVE ACOUSTIC-EMISSION ELASTIC-STRESS BEHAVIOR OF MAGNESIUM ALLOY

James H. Williams, Jr., and George P. Emerson

Prepared by
MASSACHUSETTS INSTITUTE OF TECHNOLOGY
Cambridge, Mass. 02139
for Lewis Research Center

NATIONAL AERONAUTICS AND SPACE ADMINISTRATION • WASHINGTON, D. C. • JUNE 1977

1. Report No.	2. Government Accession No.	3. Recipient's Catalog No.
NASA CR-2839		

4. Title and Subtitle	5. Report Date
CONSTITUTIVE ACOUSTIC-EMISSION ELASTIC-STRESS BEHAVIOR OF MAGNESIUM ALLOY	June 1977
	6. Performing Organization Code
7. Author(s)	8. Performing Organization Report No.
James H. Williams, Jr., and George P. Emerson	None
	10. Work Unit No.
9. Performing Organization Name and Address	
Massachusetts Institute of Technology Cambridge, Massachusetts 02139	11. Contract or Grant No. NSG-3064
	13. Type of Report and Period Covered
12. Sponsoring Agency Name and Address	Contractor Report
National Aeronautics and Space Administration Washington, D.C. 20546	14. Sponsoring Agency Code

15. Supplementary Notes

Final report. Project Manager, Alex Vary, Materials and Structures Division, NASA Lewis Research Center, Cleveland, Ohio 44135

16. Abstract

Repeated loading and unloading of a magnesium alloy below the macroscopic yield stress result in "continuous" acoustic emissions which are generally repeatable for a given specimen and which are reproducible between different specimens having the same load history. An acoustic emission Bauschinger strain model is proposed to describe the unloading emission behavior. For the limited range of stress examined, loading and unloading stress delays of the order of 50 MN/m^2 are observed, and they appear to be dependent upon the direction of loading, the stress rate, and the stress history. The stress delay is hypothesized to be the manifestation of an effective friction stress. The existence of acoustic emission elastic stress constitutive relations is concluded, which provides support for a previously proposed concept for the monitoring of elastic stresses by acoustic emission.

17. Key Words (Suggested by Author(s))	18. Distribution Statement
Acoustic emission Nondestructive testing Quality control and reliability	Unclassified - unlimited STAR Category 38

19. Security Classif. (of this report)	20. Security Classif. (of this page)	21. No. of Pages	22. Price*
Unclassified	Unclassified	40	A03

* For sale by the National Technical Information Service, Springfield, Virginia 22161

SUMMARY

Repeated loading and unloading of a magnesium alloy below the macroscopic yield stress result in "continuous" acoustic emissions which are generally repeatable for a given specimen and which are reproducible between different specimens having the same load history. An AE/Bauschinger strain model is proposed to describe the unloading emission behavior. For the limited range of stress examined, loading and unloading stress delays of the order of 50 MN/m^2 are observed and they appear to be dependent upon the direction of loading, the stress rate, and the stress history. The stress delay is hypothesized to be the manifestation of an effective friction stress. The existence of AE/elastic stress constitutive relations is concluded which provides support for a previously proposed concept for the monitoring of elastic stresses by acoustic emission [1].

INTRODUCTION

Acoustic emission (AE) refers to the generation and detection of strain waves that are produced in some materials as they undergo dynamic stresses. Most of the published work has been associated with deformation such as large-scale plasticity, crack initiation and crack propagation. Recently, a proposal by Williams and Lee [1] has shown that a characterization of the acoustic emission from macroscopically elastic metals could be utilized in a nondestructive evaluation procedure for the determination of elastic stress states*. That concept requires the acquisition of the AE activity during a specified perturbation of the original elastic stress state. Assuming the existence of a set of unique repeatable AE-stress constitutive relations, the proposal shows that information about the original stress state can be deduced. Thus, a major aspect of the development of this concept is to establish the existence and the character of AE-stress constitutive relations for elastic stress states.

Although most of the previous AE research has involved metals undergoing general macroscopic yielding, the recognition of some

---

* Note that a qualified definition of "elastic" stress is used to denote stresses below the macroscopic yield stress since microplasticity often occurs well below the macroscopic yield stress.

AE/elastic behavior has existed for at least a decade. The occurrence of AE during the unloading of a metal is mentioned briefly by Schofield [2]. Because a metal is generally believed to behave elastically during the removal of a load, this aspect of AE research is particularly intriguing. In research on AE from various steels, Kerawalla [3] and Mitchell [4] found that unload emissions occur upon repeated unloading. Kerawalla suggested that the unload emissions are due to the sudden movement of dislocation lines or tangles, but did not attempt to further specify the mechanism. The conclusion was made, however, that a great deal of the irreversible emission which occurs upon loading is associated with the yield-drop phenomenon in steel, and so, is due to the rapid breakaway of dislocations which are pinned by solute atoms of carbon and nitrogen. This conclusion appears to be in agreement with the AE studies on copper, magnesium, iron, aluminum, brass and steel by Fisher and Lally [5] who suggested that the emissions result from microscopic yield drops which are undetectable in usual tensile tests.

Agarwal [6] made a fairly comprehensive investigation of the AE behavior of aluminum, some aluminum alloys, and steel during both loading and unloading. Expanding upon a suggestion made by Sedgewick [7], Agarwal proposed that the activation of Frank-Read dislocation sources of some critical length, dependent upon the sensitivity of the AE detection system, is the source of the loading emissions.

A subsequent article by Agarwal, Frederick and Felbeck [8] showed that it is possible to relate the AE activity on loading of aluminum to its microstructure by means of the Frank-Read source activation model. A source of the unloading emissions was not proposed.

Sankar [9] investigated the unload emissions from various metals including aluminum, aluminum alloys, brass, magnesium and copper and found a correlation between these emissions and the extent of the Bauschinger effect in the metals. A later article by Sankar, Frederick and Felbeck [10] showed that a larger Bauschinger strain is accompanied by greater unload emissions, and, so it was proposed that the emissions are due to the sudden spring-back of pile-up dislocations when the load is removed, since this is generally thought to be the source of the Bauschinger effect. Also, it was proposed that the small unload emission activity found in materials with a small Bauschinger strain, such as aluminum, is a consequence of their high stacking-fault energies and resulting ease of cross-slip, such that fewer dislocations are lying in their original slip planes and, thus, cannot spring back upon a reversal of stress.

The two primary purposes of this paper are (1) to establish the existence of certain AE-stress constitutive relations for elastic stresses and (2) to emphasize the need for the standardization of AE equipment and techniques. If the former purpose is achieved, the latter need is automatically established because any constitutive

relations will depend upon the equipment and the techniques employed to obtain them. Although it is intrinsically a misnomer to state that AE-stress constitutive relations† will be equipment and technique-dependent, the relatively elementary state of current acoustic emission capability will undoubtedly make this the case for the near future. Thus, the results which are presented here must be interpreted in terms of the equipment and techniques used in the experiments.

---

† Thus, in a strict sense, any relations obtained are "pseudo constitutive" relations.

EXPERIMENTAL EQUIPMENT, MATERIAL AND PROCEDURE

The experimental equipment consisted of a hydraulic tensile loading device and acoustic emission detection (Acoustic Emission Technology) and display equipment. A schematic of the experimental system is shown in Fig. 1. The hydraulic loading device was designed such that the time-variation of the specimen load could be specified to give desired loading and unloading rates as well as maximum and minimum load values. These loading parameters were controlled by a feedback system as indicated in Fig. 1. Further details of the specimen grip assembly including specimen isolation and sensor mounting are shown in Fig. 2. A viscous couplant (AET SC-6) was used at the sensor-specimen interface and the sensor was held in contact by a force of 22 N which was exerted by the sensor loading spring.

The emissions were detected by a PZT piezoelectric sensor (AC175) having a resonant peak at 175 kHz. The AE signal was band-pass filtered (125-250 kHz) and the total system amplification was maintained at 100 db. The minimum detectable signal by the system for a constant threshold voltage of 0.6 V (after amplification) corresponded to a sensor stress of 1.9×10^{-9} MN/m^2. Extensive details relating to the feedback parameters, system rates and loading capabilities, and system calibration are given in [11].

The test specimens were made from a wrought magnesium alloy (AZ31B-F). The gage section of the specimens was a solid circular cylinder having a length of 7.62×10^{-2} m and a diameter of 7.62×10^{-3} m. The heat treatment and some physical properties of the magnesium are given in Table 1.

Table 1

Heat treatment and some physical properties of magnesium alloy specimens

Material	Magnesium (AZ31B-F)
Heat Treatment	260° C for 20 min; air cooled
Hardness Before Heat Treatment (Rockwell scales)	R_F=57
Hardness After Heat Treatment (Rockwell scales)	R_F=52
0.2% Offset Tensile Yield Strength (MN/m^2)	183.4
Ultimate Tensile Strength (MN/m^2)	366

The experimental procedure may be described by the following set of statements:

1. Load the the specimen for one hour to a stress, σ_{max}, which is below the yield stress. The stress σ_{max} represents the maximum stress reached in the entire loading history.

2. Unload the specimen to a lower stress, σ_{lower}, for 10 sec, then reload it to an upper stress, σ_{upper}, for 20 sec.

3. After repeating this 30 sec cycle four times, the value of σ_{upper} is decreased, and four more unload-load cycles are performed.

4. This procedure is repeated using successively smaller upper stress levels until no emissions are recorded. Then the procedure is repeated using successively larger upper stress levels until σ_{max} is reached again.

Three types of tensile tests were conducted using the general procedure described above. These tests are characterized as follows:

1. Full Unload Tests: σ_{upper} varies as indicated and σ_{lower} is always zero. This type of test is illustrated in Fig. 3.

2. Partial Unload Tests: σ_{upper} varies as indicated and σ_{lower} varies in accordance with $\sigma_{lower} = \sigma_{upper} - \Delta\sigma$, where $\Delta\sigma$ is a stress increment that is maintained constant throughout the test.

3. Stress Rate Tests: A range of loading and unloading rates is used between σ_{upper} which is constant throughout the test and σ_{lower} which is zero throughout the test.

For all tests, the cumulative AE loading count (ΣE_L) and the cumulative AE unloading count (ΣE_U) were recorded. Also, the AE signals were observed on an oscilloscope which provided qualitative information.

RESULTS AND DISCUSSION

The major emphasis of the results and discussion section is the presentation of experimentally reproducible AE/elastic stress constitutive behavior. Before presenting those results, however, a brief discussion of the AE which occurs during the initial loading as well as a description of "burst" and "continuous" emissions observed during the tests will be given.

Characteristics of First-Load AE

During the first loading of the specimen, prolific acoustic bursts of 2 to 7 volt amplitude (after 100 db amplification) are generated and continue for up to one hour if the stress is held constant at its maximum value. The cumulative loading emission count (ΣE_L) versus time for specimen #1 is shown in Fig. 4. If the specimen is unloaded while these emissions are occurring, the bursts stop. For tests conducted during time periods of the order of one hour, these bursts behave according to the so-called Kaiser effect. However, if the specimen is left at zero load for a week or more, loading it to a stress below σ_{max} results in burst emissions, although the activity declines more rapidly than during the first load.

The time-dependent character of the burst emissions suggests that a thermally activated process, such as creep, controls their

generation. This transient creep effect is often explained by an "exhaustion" theory whereby sources of slip, such as dislocations, encounter barriers which cannot be overcome unless an activation stress which is greater than the externally applied stress is imposed. The energy required to achieve the activation stress may be supplied by the inherent thermal vibrations in the crystal. Because there is a finite number of such slip sources, each with its own activation stress, the creep rate, which is determined by the probability of the sources being thermally activated, decreases with time as the sources with the lower activation stresses are used up, or "exhausted". One type of slip source which could be used to explain the burst emissions, and which is consistent with the mechanism proposed in [8] is the well-known Frank-Read dislocation mill.

After the burst emissions have subsided at a given σ_{max}, subsequent loading and unloading to stresses below σ_{max} result in a different type of emission. For these loading and unloading cycles the emission signal appears as a general rise of the inherent noise in th AE monitoring system. However, as discussed in [11], these "continuous" emissions could be composed of many bursts of smaller amplitude occurring at a rate greater than $1/\tau_d \approx 10^4$/sec, where τ_d is the characteristic decay time of the sensor-amplifier system during "ring-down". Thus, the terms "burst" and "continuous" which are frequently used in AE terminology are dependent upon both the AE source and the AE monitoring system.

Full Unload Tests

Following the loading sequence illustrated in Fig. 3, the resulting ΣE_U and ΣE_L versus σ_{upper} for two magnesium specimens are shown in Figs. 5 and 6. The mean (indicated by points) and the standard deviation (indicated by brackets) for four successive counts are plotted versus σ_{upper}. These values are plotted separately for the decreasing and increasing loading patterns where the arrows indicate the sequence of the tests. It is important to note that sepcimens #1 and #2 are different specimens from the same batch of material and that the specimens were mounted and tested on different days.

Several significant comments can be made concerning Figs. 5 and 6.

1. Although there are some differences between the plots for the two specimens, both the loading and the unloading emission count graphs are very similar for each type of test.

2. The large standard deviations in the loading emissions (Fig. 6) at the highest upper stress level ($\sigma_{upper} = \sigma_{max}$) are a direct consequence of the burst emissions which occur whenever the specimen is loaded up to σ_{max}. (If the stress is less than σ_{max}, the emissions cease as soon as the stress on the specimen ceases to change.)

3. The emissions are dependent upon the loading pattern; that is, they are less for a decreasing loading pattern than for an increasing loading pattern.

4. The dashed lines in Fig. 5 represent full unload tests for a smaller value of σ_{max}, where σ_{max} is the maximum stress in the entire post-heat treatment history of the magnesium. The loading emissions (Fig. 6) for this same σ_{max} are erratic and are an order of magnitude less than the unload emissions. Thus, these emission characteristics are a function of the maximum stress in the magnesium's history.

Most of the deviation observed in the unload and load emission counts at the higher stress levels less than σ_{max} is due to an effect illustrated in Fig. 7, which shows the E_L and E_U for repeated loading and unloading of a magnesium specimen between σ = 0 and 154 MN/m^2. Each point in Fig. 7 represents the cumulative count for one load or one unload. It can be seen that the counts vary slowly with the number of cycles and appear to level-off after about 30 cycles.

Partial Unload Tests

Fig. 8 shows the results of the partial unloading and loading tests on specimen #2 for $\Delta\sigma$ = 96.5 MN/m^2. Although the same tests were performed on specimen #1, these tests are not presented because they show the same general trends [11].

A question raised by the results shown in Fig. 8 is why do both the loading and unloading cumulative emission counts for a given change in stress $\Delta\sigma$, decrease with an increasing upper stress level, σ_{upper}. If the total emission activity is assumed to be related to the Bauschinger strain β, as suggested in [10], an explanation of these trends would depend upon how β varies with $\Delta\sigma$ and σ_{upper}.

Unfortunately, most research on the Bauschinger effect has involved plastic strains in excess of 0.1%. The reason for using such large strains has generally been the difficulty involved in obtaining accurate measurements of the Bauschinger strain β, for plastic strains below 0.1%. Some of the behavior observed for these large strains will be extrapolated into the small strain region with the understanding that the results obtained may be used to indicate trends only.

Some of the parameters usually used to quantify the Bauschinger effect are illustrated in Fig. 9 which shows a typical stress-strain curve of a metal which exhibits this effect. σ_p is a "pre-stress" imposed on the metal before reverse loading; β is the difference between the measured strain during unloading and the elastic strain which would result in a material not exhibiting the Bauschinger effect (dashed line); and σ is the stress level at which this strain difference is measured. The stress σ is usually taken to be a compressive stress whose magnitude is some fraction η, of the pre-stress; that is, $\sigma = -\eta\sigma_p$. The following nondimensional constitutive relationship between β, σ_p and σ is proposed:

$$(\beta/\beta_o) = f(\sigma/\sigma_p)\ g(\sigma_p/\sigma_o) \qquad (1)$$

The function $f(\sigma/\sigma_p)$ describes the shape of the unloading curve of β versus σ, normalized with respect to σ_p, for a typical unloading. The function $g(\sigma_p/\sigma_o)$ defines how the magnitude of β varies with the pre-stress σ_p, normalized with respect to some constant stress σ_o. β_o is another normalizing constant which defines the actual magnitude of the Bauschinger strain for a given material.

Fig. 10 illustrates some typical shapes of these functions which are based on experimental results [12-14]. Let

$$f\left(\sigma/\sigma_p\right) = \left(1 - (\sigma/\sigma_p)\right)^n \tag{2}$$

For $n = 1$ this results in a straight line and as $n \to \infty$, the curve sags in towards the coordinate axes (curve A, Fig. 10 (a)). Although the exact shape of this curve is not known, especially for small pre-stresses, this general shape appears to be a good approximation. Also, note that for $0 < n < 1$ the curve bows out from the origin, which does not appear to be a reasonable approximation [12-14].

The variation of β with the pre-stress, σ_p, defined by the function $g(\sigma_p/\sigma_o)$, has taken the approximate forms indicated by the curves A, B and C in Fig. 10 (b) through the work of Wooley [12], Buckley and Entwistle [13], and Deak [14], respectively. Both of latter two indicate that some minimum pre-stress, defined as σ_o, must

be reached before the Bauschinger effect is observed. Thus, let

$$g\left(\sigma_p/\sigma_o\right) = \left((\sigma_p/\sigma_o)^m - 1\right)^{1/m} \tag{3}$$

For m = 1 the result is a straight line (curve C), whereas for m > 1 the curve (curve B) bends down closer to the asymptote defined by the 45° line. As $m \to \infty$ the curve approaches the 45° line (curve A). Again the exact value of m is not known for small σ_p, but this functional form appears consistent with the empirical results which have been referenced.

To apply these assumed functional relationships to the results of the partial unload tests, let the pre-stress be the upper stress level; that is, $\sigma_p = \sigma_{upper}$; and let $\sigma = \sigma_p - \Delta\sigma$. Combining these concepts with equations (1), (2) and (3) gives

$$(\beta/\beta_o)^m = (\Delta\sigma/\sigma_o)^{nm}\left[1 - (\sigma_o/\sigma_p)^m\right](\sigma_o/\sigma_p)^{m(n-1)} \tag{4}$$

Plots of $(\beta/\beta_o)^m \cdot (\sigma_o/\Delta\sigma)^{mn}$ versus (σ_p/σ_o) for various values of $n \geq 1$ and $m \geq 1$ are shown in Fig. 11. Note that

1. For any values of $n > 1$ and $m > 1$ the shape of β versus σ_p for a given $\Delta\sigma$ does not change appreciably;
2. β is not defined for $\sigma_p < \sigma_o$: that is, no Bauschinger strain is expected in this region; and
3. For a given $\Delta\sigma$, β tends to decrease with increasing σ_p for the larger values of σ_p.

If the correlation is made, between β and ΣE_U, it can be seen than any of the curves in Fig. 11 for $n > 1$ indicates a decreasing emission count for increasing upper stress levels, as observed in the partial unload tests. In addition, a similar result is expected for the partial loading tests, except that the loading portion of the stress-strain hysteresis loop is used with the effective pre-stress equal to the lower stress level.

Although this derivation is not a proof either that the Bauschinger effect is the cause of the unloading emissions or that the cumulative emission count is directly related to the Bauschinger strain, the similar trends observed do indicate some correlation between the proposed model and the experimental results. In addition, due to the wide range of values of m and n for which the trends in the model apply, a range of forms of the functions $f(\sigma/\sigma_p)$ and $g(\sigma_p/\sigma_o)$ which are similar to those shown in Fig. 10 will result in the same trends.

Stress Delay and Stress Rate Tests

Fig. 12 shows a typical chart recorder plot for an unloading test. A "stress delay" is observed in loading and in unloading, denoted by σ_{DL} and σ_{DU}, respectively. That is, the emission activity does not begin during either loading or unloading until a definite loading or unloading change in stress has occurred. Similar behavior has been reported for unload emissions in steel and aluminum [3,4 and 6]. The stress delays observed during the partial unload tests ($\Delta\sigma$ = 96.5 MN/m^2) for both specimens #1 and #2 in loading and unloading are shown in Fig. 13. The following observations about Fig. 13 are made:

1. By far the most significant aspect is the close similarity of the results from specimens #1 and #2.
2. There appears to be a loading pattern dependency which is more pronounced for the unloading stress delay.
3. The unloading stress delay displays a pattern which tends to decrease with decreasing σ_{upper}.
4. The loading and unloading stress delays are approximately same magnitude for the range of σ_{upper} investigated.

The direct importance of the stress delay to the trigger concepts in [1] strongly indicates the value of clearly defining the functional dependence of the stress delays upon σ_{upper}, σ_{max} and the stress rate.

The stress delays for loading and unloading at various stress rates are shown in Fig. 14. There is a trend towards larger delays at lower stress rates. Also, at the higher stress rates, the stress delay for loading and unloading are nearly equal (although this may

be due, in part, to a system saturation effect [11]). The increase in the stress delay at the lower stress rates may reflect the fact that although AE activity may begin at all rates after a constant stress delay, the signal does not exceed the threshold until some time later. Thus, at the lower stress rates where the total emission activity is generally smaller, this effect will manifest itself as a larger stress delay.

The existence and behavior of the stress delay suggest that it is the result of an effective friction stress. Considering a dislocation under the influence of an externally applied shear stress τ_{A1}, and back shear stress τ_B, due either to a pile-up of other dislocations or to intersections with obstacles (for example, forest dislocations or precipitates), the total shear stress on the dislocation is

$$\tau_{A1} - \tau_B = \tau_f \tag{5}$$

where τ_f is the effective friction stress. When the stress is reversed, reverse flow occurs when the stress on the dislocation becomes

$$\tau_{A2} - \tau_B = -\tau_f \tag{6}$$

where τ_{A2} is the applied shear stress at which reverse flow occurs. The required change in the externally applied shear stress is

$$\tau_D = (\tau_{A1} - \tau_{A2}) = 2\tau_f \ . \qquad (7)$$

Assuming flow will occur first in the most favorably oriented grains

$$\tau_f = \frac{1}{2}\tau_D = \frac{1}{4}\sigma_D \approx 15 \text{ MN/m}^2 \qquad (8)$$

where a typical value of 60 MN/m^2 has been taken (See Fig. 14.)

A probable major contribution to the stress delay can be attributed to the resistance to dislocation motion due to solute atoms. The shear stress, τ_s, required to move a dislocation through the lattice of a solution hardened alloy can be estimated by [15]

$$\frac{\tau_s}{\mu} = \frac{1}{2}\,\varepsilon^{\frac{4}{3}}\,C\left[\frac{C^{\frac{2}{3}}\,(\ln C)^4}{\alpha}\right]^{\frac{1}{3}} \qquad (9)$$

where, μ = shear modulus,

ε = lattice misfit parameter $\simeq (r_a/r_b)-1$,

r_a = solute atom radius,

r_b = solvent atom radius,

C = volume concentration of solute,

α = a factor $\simeq$ 0.5.

Table 2

Physical parameters used in estimating the friction stress in the AZ31B-F alloy due to solution hardening

	Mg	Al	Zn	Mn
Weight Concentration*	---	0.03	0.01	0.002
Density (gm/cm^3)**	1.74	2.699	7.133	7.43
Volume Concentration	---	0.0193	0.0024	0.00047
Atomic Radius ($\mathring{A}$)***	1.598	1.431	1.332	1.12
$\lvert\varepsilon\rvert$	---	0.105	0.166	0.299
(τ_s/μ)	---	1.56×10^{-3}	3.96×10^{-4}	1.63×10^{-4}

*Metals Handbook, [16], p. 1106

**Ibid., pp. 44-45

***Ibid., pp. 50-51

Summing the contributions in Table 2, equation (9) becomes

$$\frac{\tau_s}{\mu} \approx 2.1 \times 10^{-3} \qquad (10)$$

This value should be compared with

$$\frac{\tau_f}{\mu} \approx 9.1 \times 10^{-4} \qquad (11)$$

which is derived from equation (8) where $\mu = 1.65 \times 10^4$ MN/m^2 for magnesium. Although the result in equation (10) is larger than the observed quantity in (11), the discrepancy may be due in part to the neglection of the precipitation of a certain amount of the alloying elements, which would effectively result in smaller solute concentration, C. Also, Cottrell [15] has noted that equation (9), which was derived neglecting thermal effects, tends to overestimate the hardening effect observed at room temperature, since thermal fluctuations may assist dislocations in overcoming barriers.

If a more thorough investigation of the stress delay indicates that it is essentially constant as assumed above, then the solution hardening effect discussed is likely to play a major role in determining its value. On the other hand, if σ_D depends on σ upper, the stress rate, and in particular, σ_{max} as it apparently does for steel, then the interaction between mobile and forest dislocations (which would be rearranged by stain hardening) is likely to be a major source of the stress delay effect.

Finally, in returning to the discussion on the AE/Bauschinger strain model, the range of forms which may be assumed for $f(\sigma/\sigma_p)$ and $g(\sigma_p/\sigma_o)$ admits a stress delay without alteration to the proposed model. Note that the stress delay can be considered as a region of stress just below $\sigma/\sigma_p = 1$ for which $f(\sigma/\sigma_p) = 0$. This effect simply accentuates the "sagging" of the $f(\sigma/\sigma_p)$ curve toward the axes. Curve B in Fig. 10 (a) illustrates a suitable $f(\sigma/\sigma_p)$ which accommodates the stress delay.

CONCLUSIONS

Experimental results characterizing the AE/stress behavior of elastically stressed AZ31B-F magnesium have been presented. During the first loading, many "burst" emissions are generated and continue for up to one hour if the maximum load is maintained. Subsequent repeated loadings and unloadings generate "continuous" emissions during both loading and unloading. These "continuous" emissions are cycle-dependent in that repeated loadings and unloadings result in cumulative emission counts which vary with the number of cycles. However, a shakedown phenomenon occurs since after about 30 cycles the cumulative counts remain constant and are highly repeatable.

For a given change in stress the resulting cumulative counts in loading and unloading generally decrease with increasing upper stress levels, at least for the range of upper stress levels investigated. An empirically derived model of the Bauschinger effect indicates a similar trend. A stress delay of approximately 50 MN/m^2 is observed in the continuous emission which is quite reproducible for different specimens with the same history. Both the loading and unlaoding stress delays appear to be functions of the direction of loading, the stress rate and the loading history. A form of dislocation friction stress due to a solution hardening effect is suggested as a major source of the stress delay.

Thus, the existence of AE/elastic stress constitutive relations has been demonstrated. Despite this important observation, the data which have been presented must be interpreted in terms of trends only as the specific values associated with them depend upon the experimental apparatus used. Therefore, the standardization of AE equipment and techniques represents an endeavor of distinct importance in the development of acoustic emission utilization.

REFERENCES

1. Williams, J. H., Jr., and Lee, S. S., "Monitoring of Elastic Stresses by Acoustic Emission", International Journal of Nondestructive Testing, 1977.

2. Schofield, B. H., "Acoustic Emission Under Applied Stress", Technical Documentary Report No. ASD-TDR-63-509, Part II, Wright Patterson Air Force Base, May 1964.

3. Kerawalla, J. N., "An Investigation of the Acoustic Emission From Commercial Ferrous Materials Subjected to Cyclic Tensile Loading", Doctoral Thesis, The University of Michigan, October 1965.

4. Mitchell, L. D., "An Investigation of the Correlation of the Acoustic Emission Phonomenon With the Scatter in Fatigue Data", Doctoral Thesis, The University of Michigan, October 1965.

5. Fisher, R. M., and Lally, J.S., "Microplasticity Detected by an Acoustic Technique", Canadian Journal of Physics, Vol. 45 (1965), pp 1147-1159.

6. Agarwal, A. B. L., "An Investigation of the Behavior of the Acoustic Emission From Metals and a Proposed Mechanism For Its Generation", Doctoral Thesis, The University of Michigan, 1968.

7. Sedgewick, R. T., "An Investigation of Acoustic Emission From Coated and Uncoated Ionic Crystals", Doctoral Thesis, Michigan State University, 1965.

8. Agarwal, A. B. L., Frederick, J. R. and Felbeck, D. K., "Detection of Plastic Microstrain in Aluminum by Acoustic Emission", Metallurgical Transactions, Vol. 1, April 1970, pp. 1069-1071.

9. Sankar, N. G., "Unload Emission Behavior of Materials and Its Relation to the Bauschinger Effect", Doctoral Thesis, The University of Michigan, 1969.

10. Sankar, N. G., Frederick, J. R., and Felbeck, D. K., "Acoustic Emission From Metals During Unloading and Its Relation to the Bauschinger Effect", Metallurgical Transactions, Vol. 1, December 1970, pp. 2979-2980.

11. Emerson, G. P. and Williams, J. H., Jr., "Acoustic Emission from Elastically Stressed Metals", Report for NASA Grant No. NSG-3064, Dept. Mech. Eng., M.I.T., Cambridge, Mass., August 1976.

12. Wooley, R.L., "The Bauschinger Effect in some Face-centered and Body-centered Cubic Metals", Philosophical Magazine, Series 7, Vol. 44, 1953, pp. 597-618.

13. Buckley, S. N., and Entwistle, K. M., "The Bauschinger Effect in Super-Oure Aluminum Single Crystals and Polycrystals", Acta Metallurgica, Vol. 4, July 1965, pp. 352-361

14. Deak, G. I., "A Study of the Causes of the Bauschinger Effect", Doctoral Thesis, M.I.T., Cambridge, Mass., 1961.

15. Cottrell, A. H., Dislocations and Plastic Flow in Crystals, Oxford University Press, London, 1953.

16. Metals Handbook, ed. 8, Vol. 7, "Properties and Selection of Materials", American Society for Metals, Metals Park, Ohio, 1967.

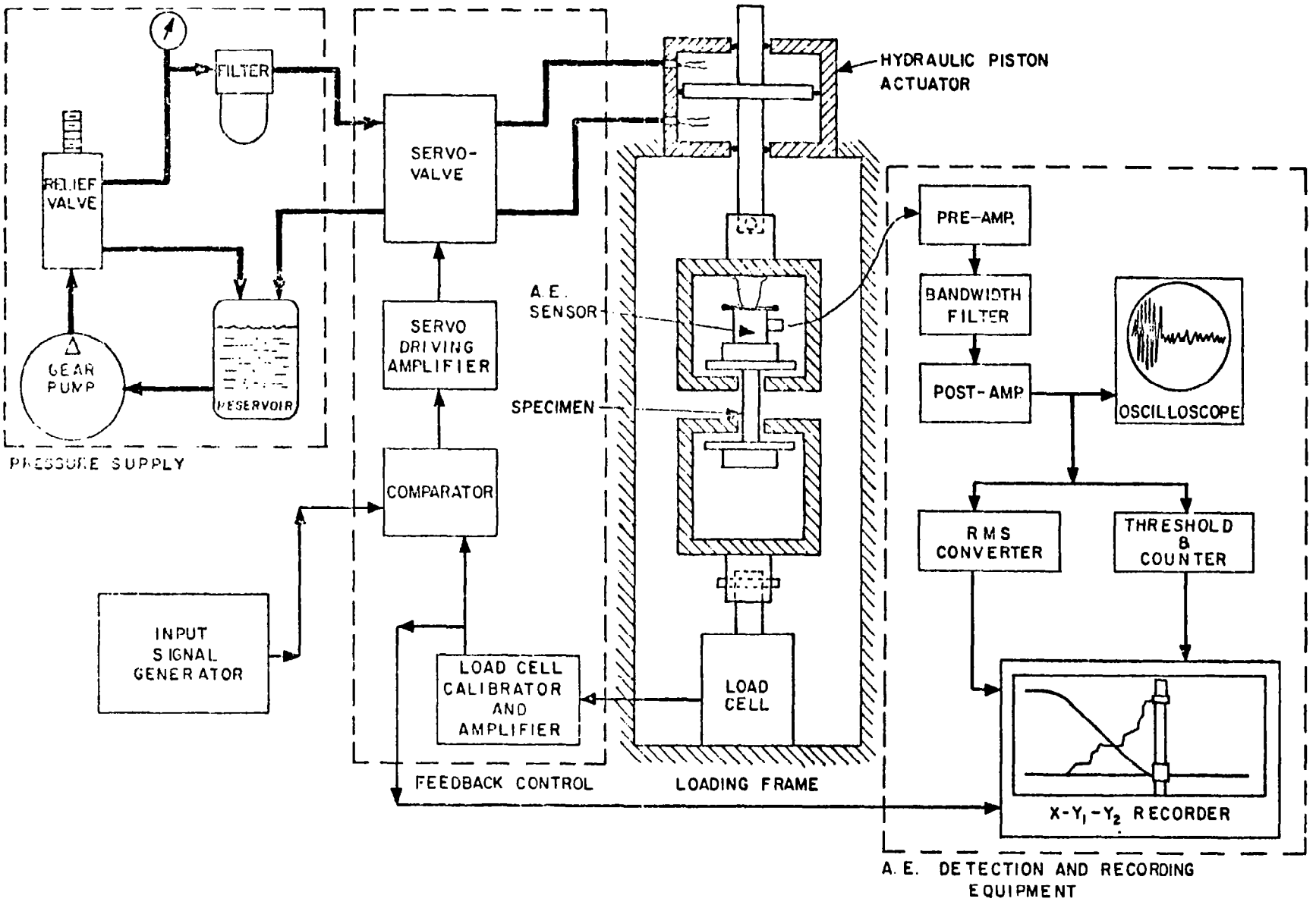

Fig. 1 Schematic of Acoustic Emission Loading and Monitoring System.

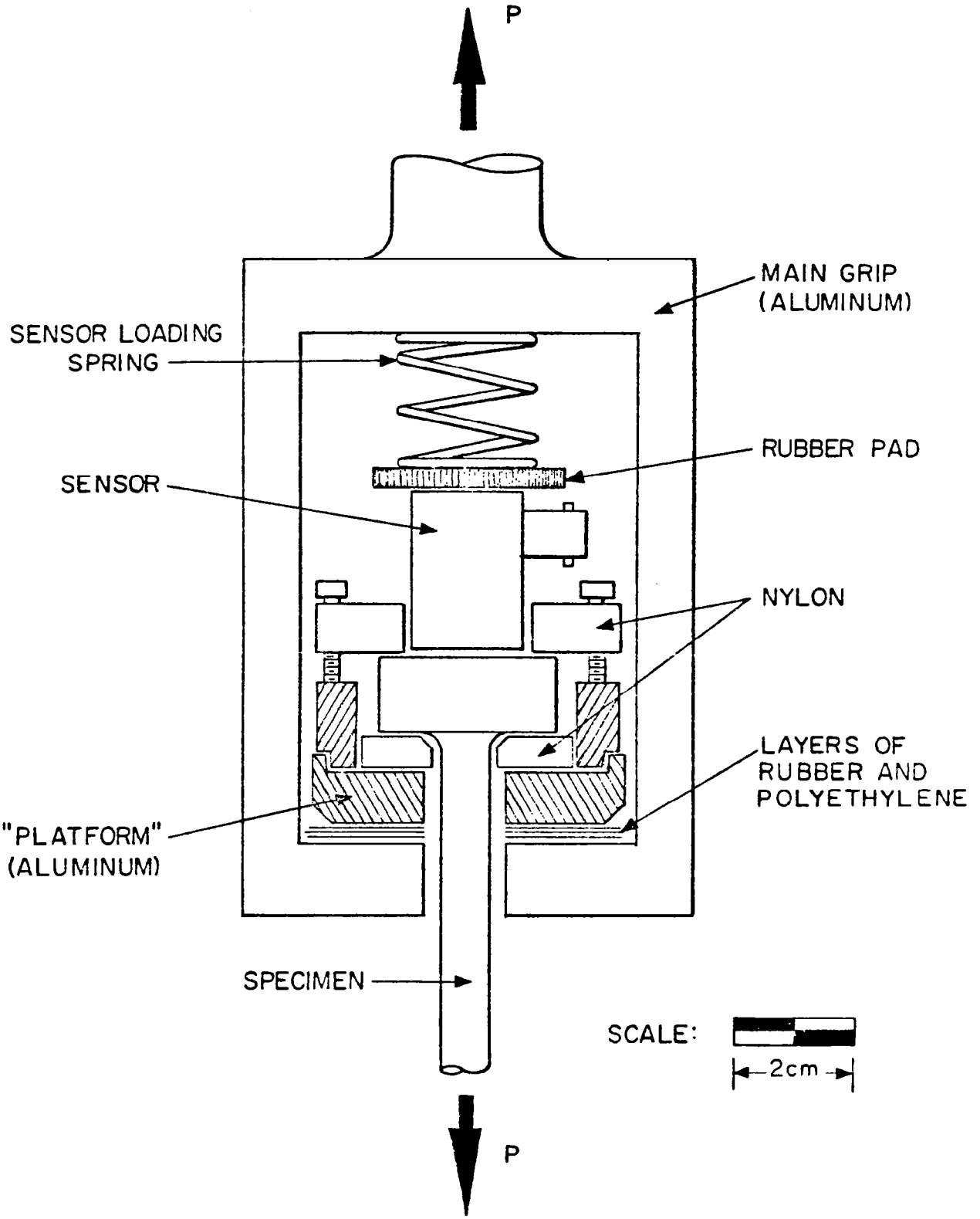

Fig. 2 Schematic of Tensile Specimen Grip Assembly and Acoustic Emission Sensor.

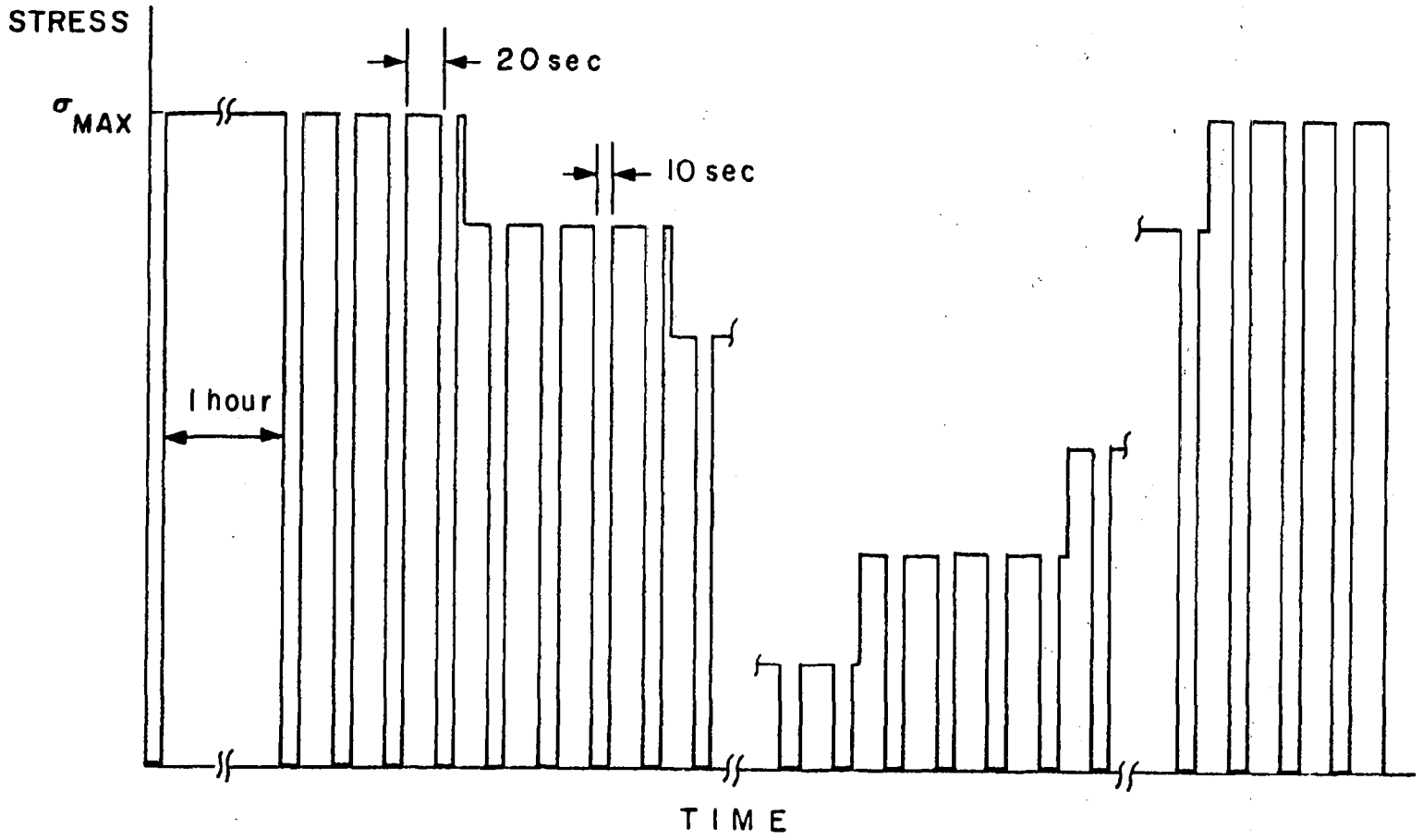

Fig. 3 Typical Specimen Loading-Unloading Sequence for Full Unload Tests.

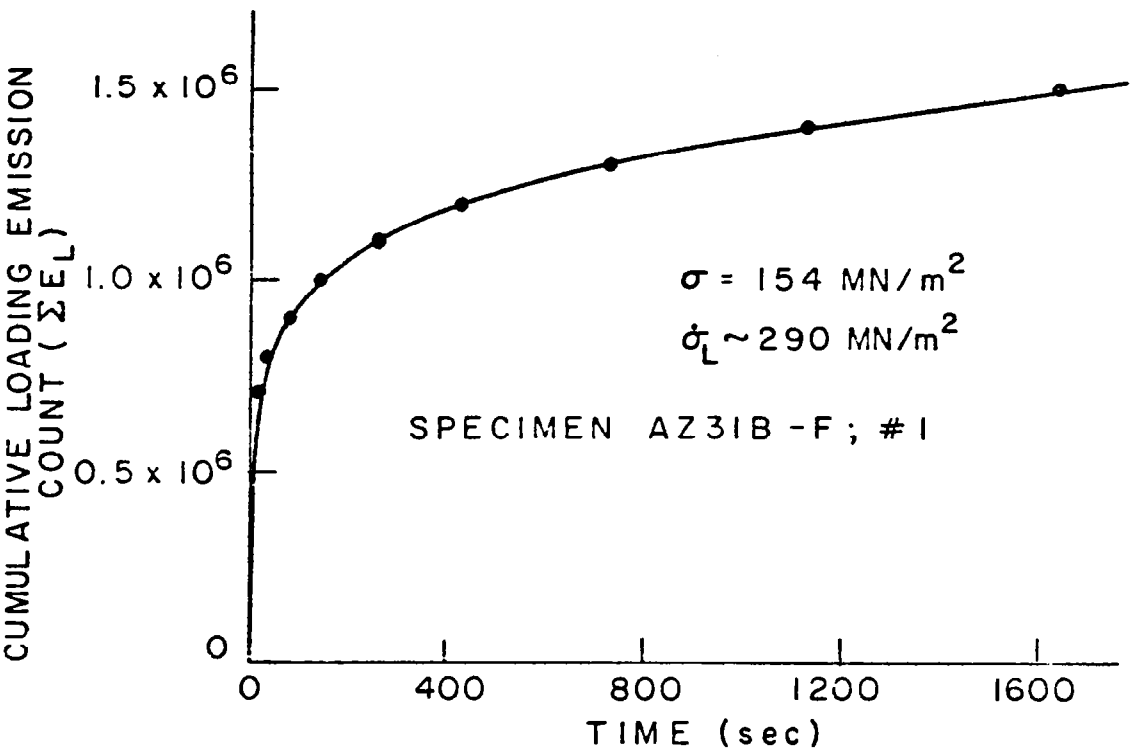

Fig. 4 Cumulative Loading AE Counts for First Loading of a Magnesium Specimen.

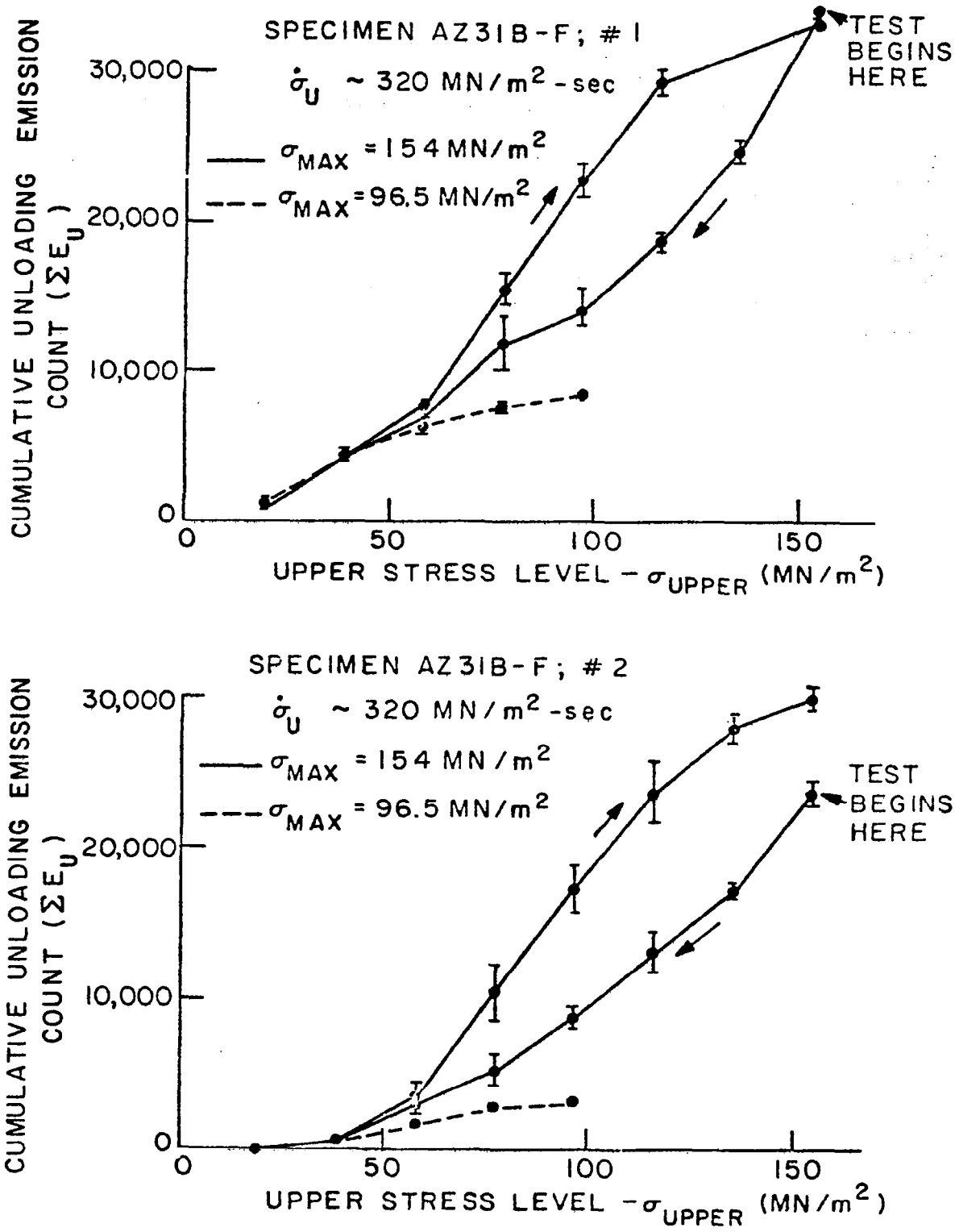

Fig. 5 Full Unloading AE from Two Magnesium Specimens.

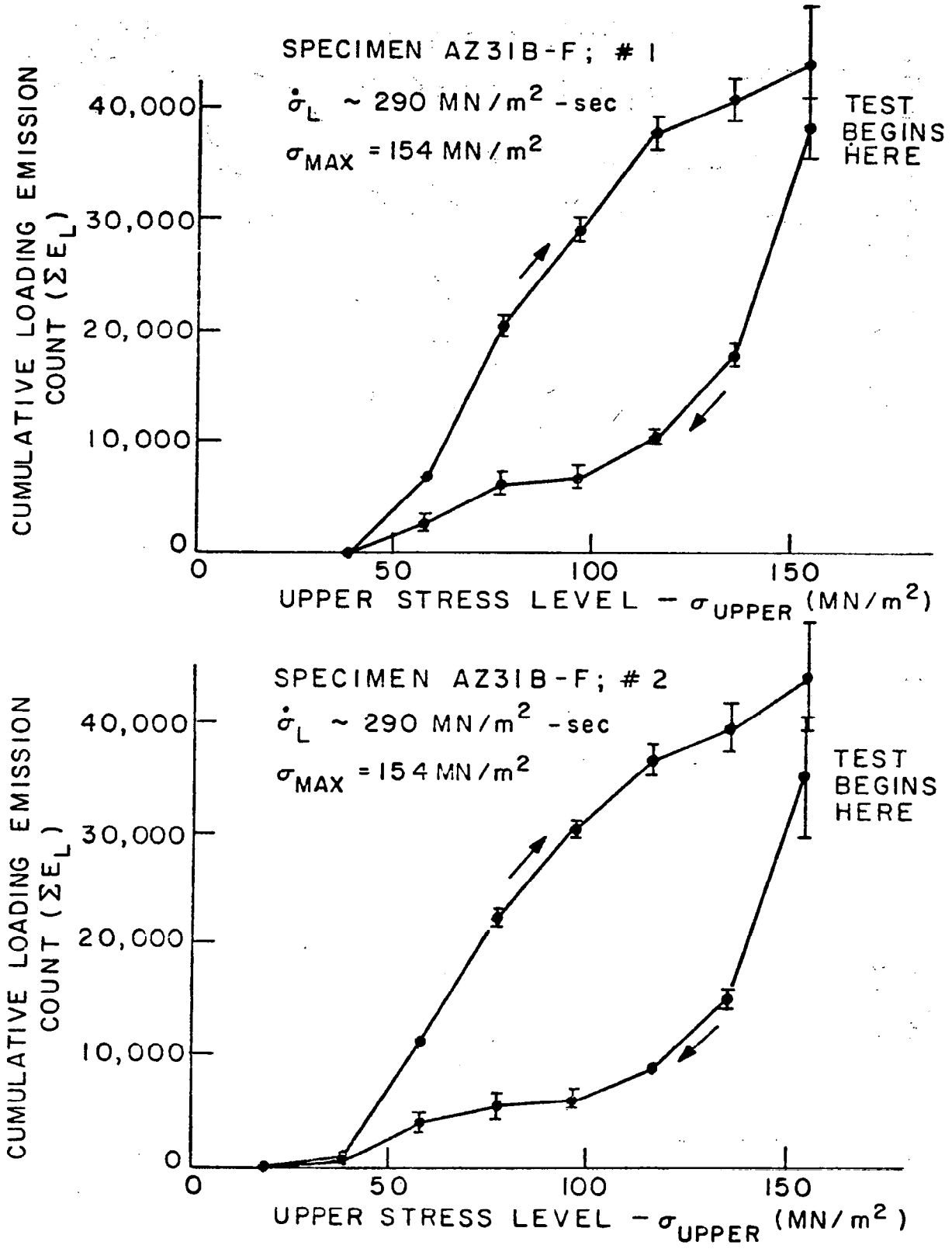

Fig. 6 Full Loading AE from Two Magnesium Specimens.

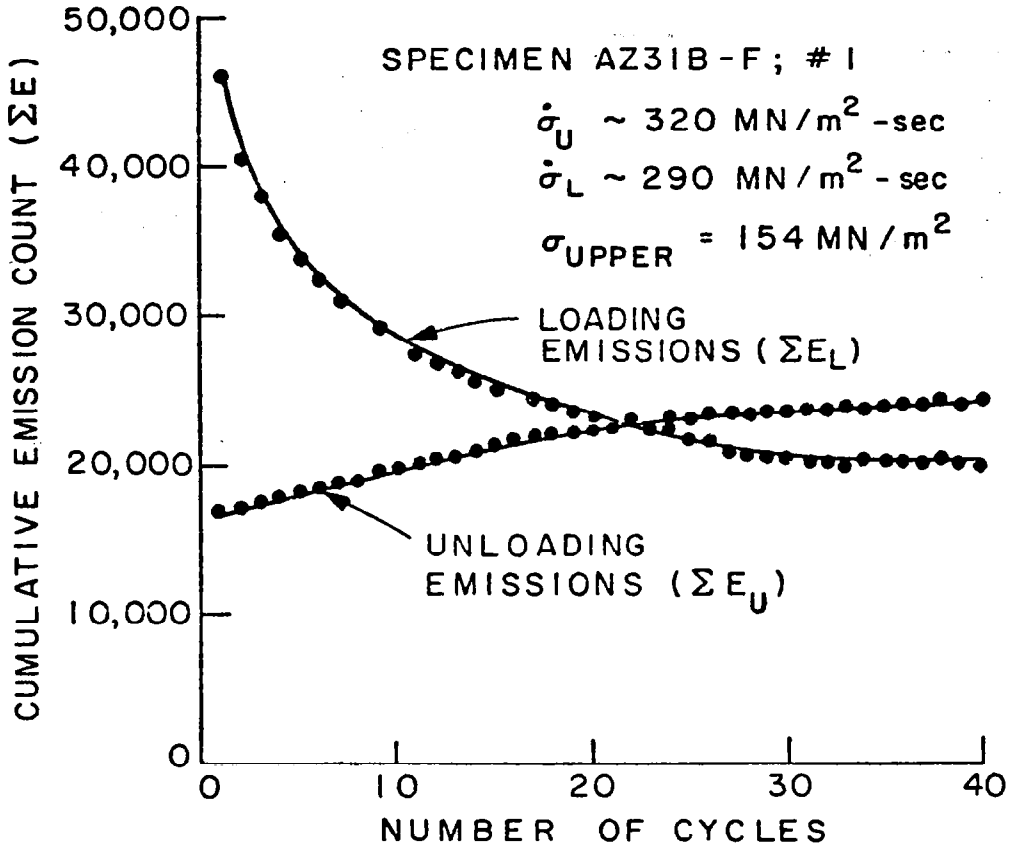

Fig. 7 Cumulative Loading and Unloading AE for Repeated Load-Unload Cycles.

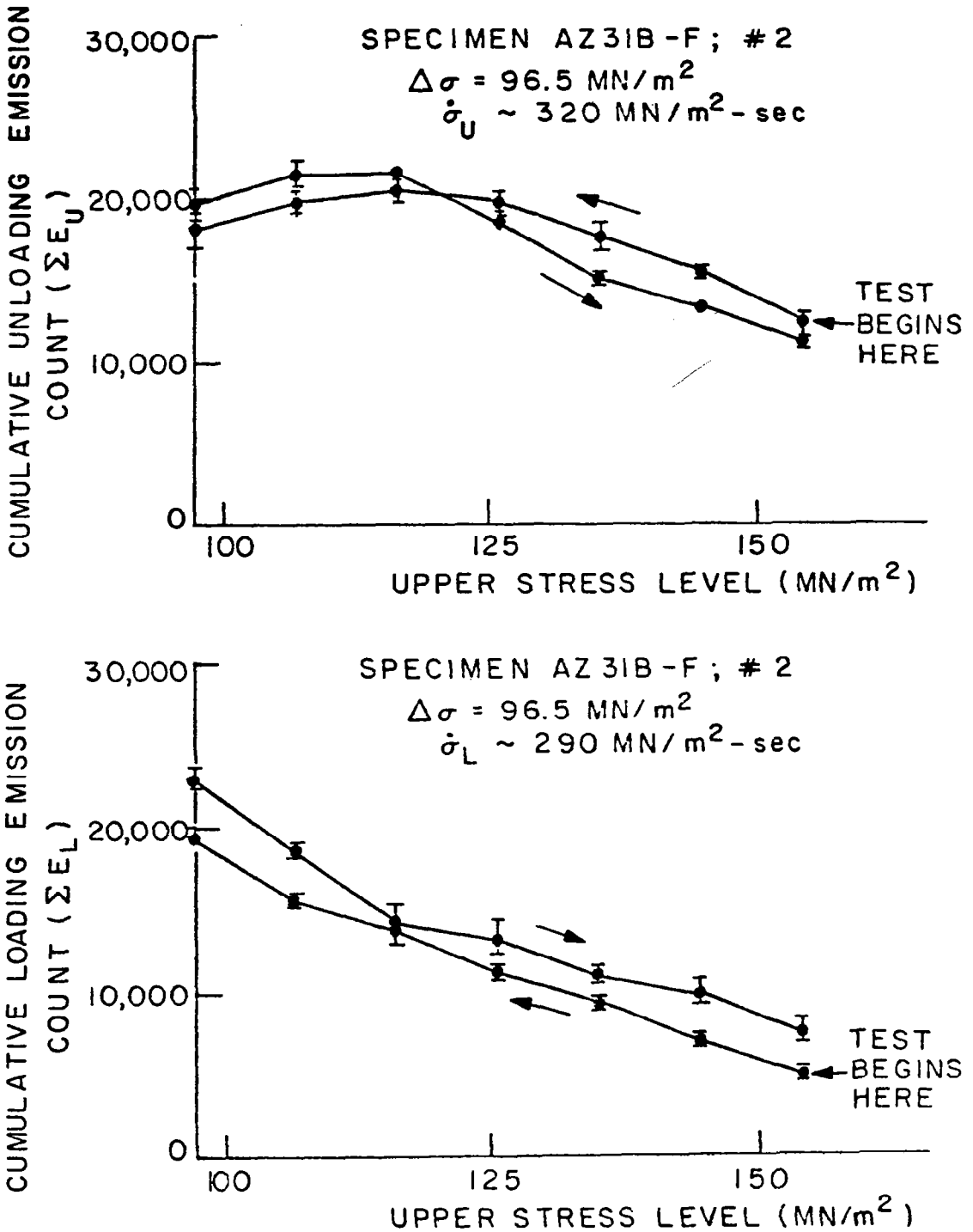

Fig. 8 Partial Unloading and Loading AE from Magnesium Specimen #2.

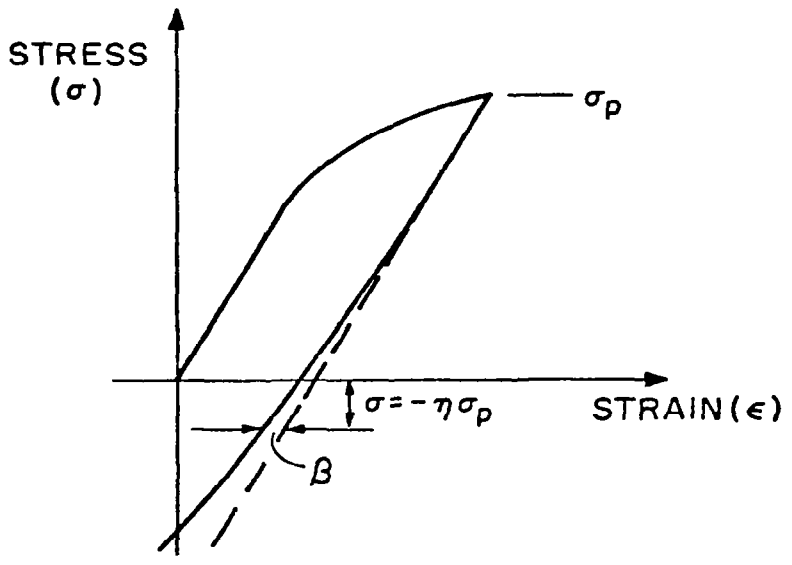

Fig. 9 Typical Stress-Strain Curve for a Metal Exhibiting the Bauschinger Effect.

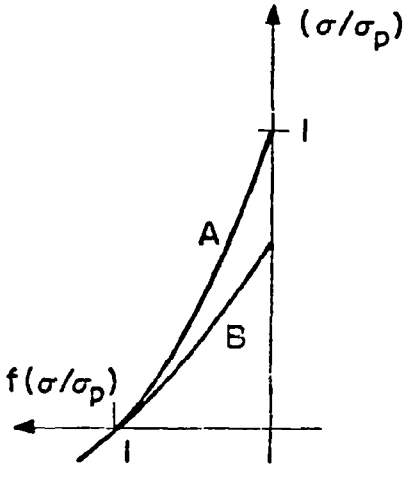

Fig. 10 (a) Generic $f(\sigma/\sigma_p)$ Functions for AE/Bauschinger Strain Model

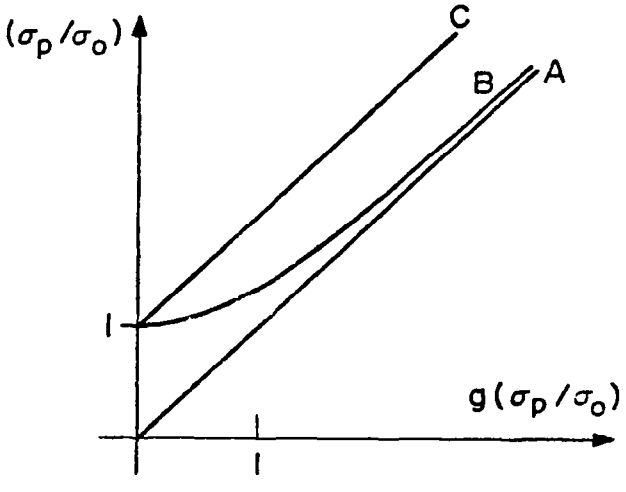

Fig. 10 (b) Generic $g(\sigma_p/\sigma_o)$ Functions for the Proposed AE/ Bauschinger Strain Model.

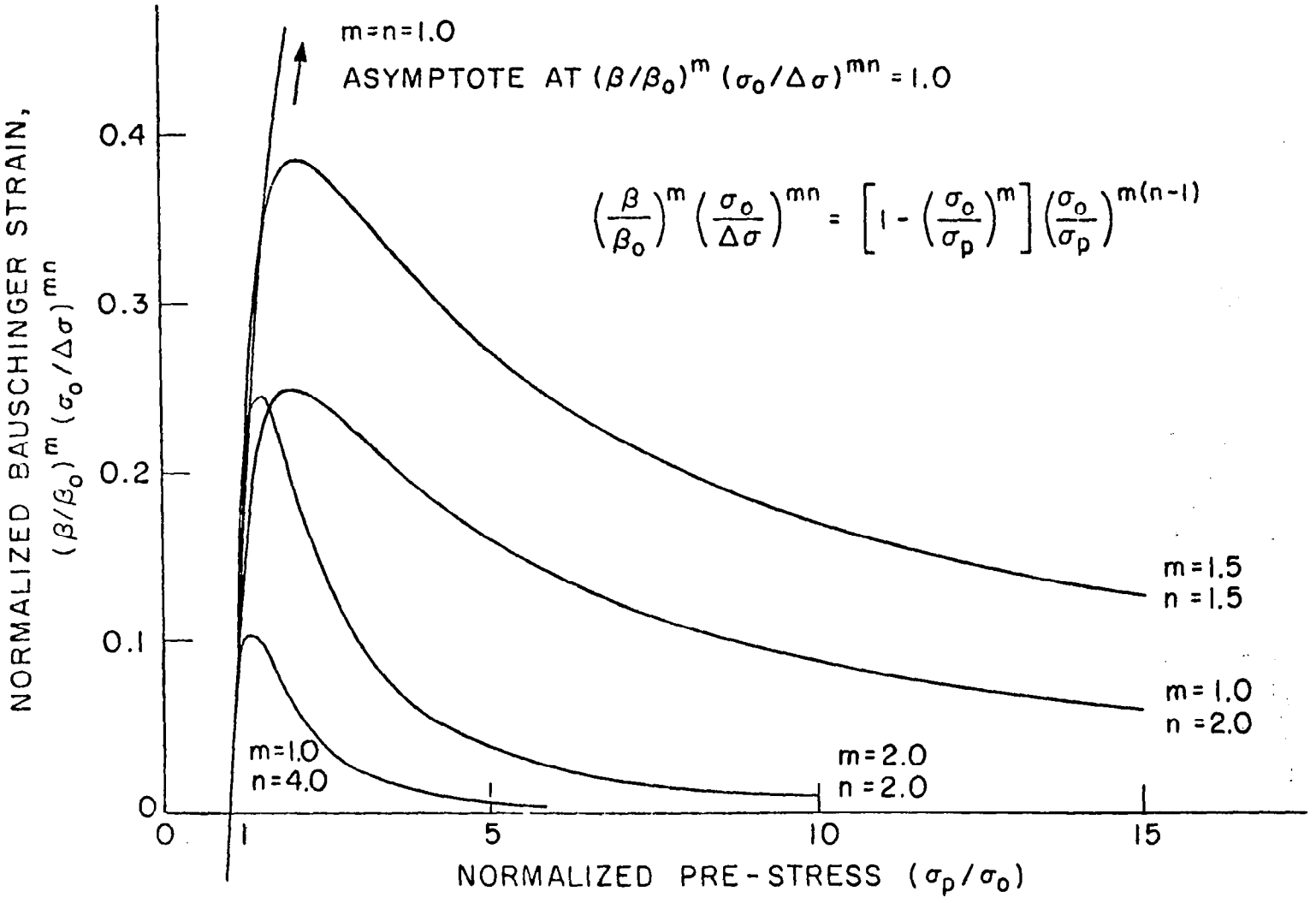

Fig. 11 Normalized Curves for the Proposed AE/Bauschinger Strain Model for a Given $\Delta\sigma$ for Various Values of m and n.

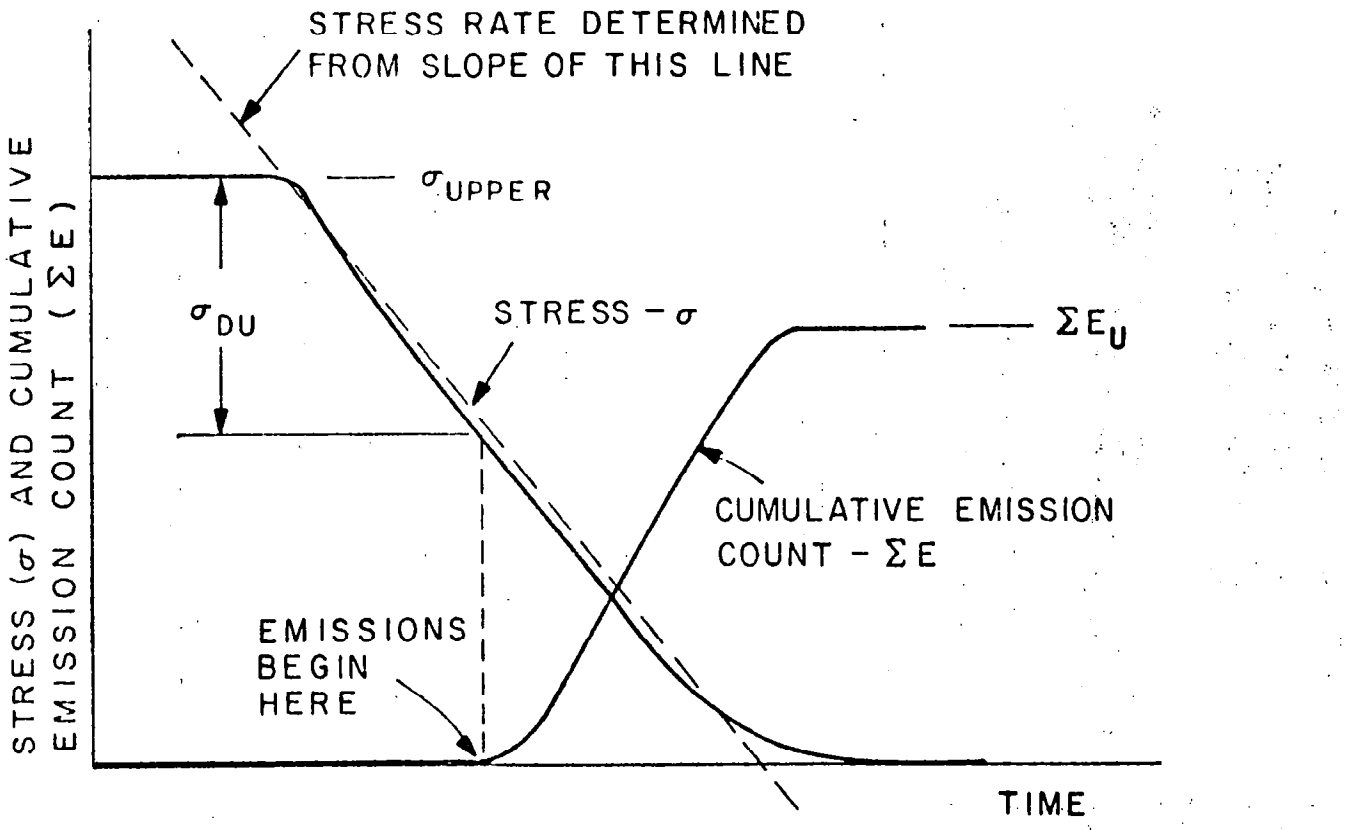

Fig. 12 Generic Chart Recorder Plot for Unloading Test Indicating Stress Delay and Stress Rate.

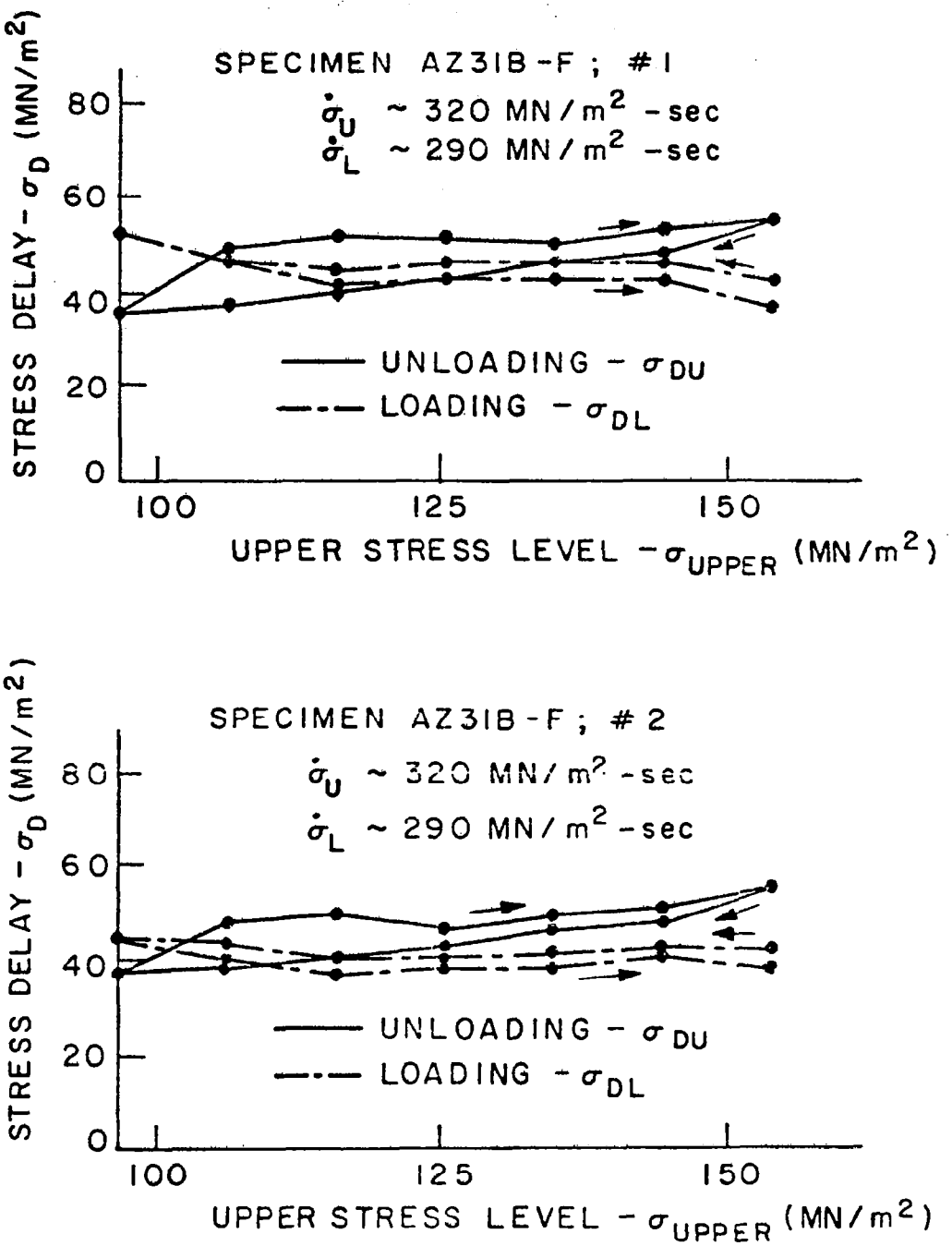

Fig. 13 Stress Delays Observed During Partial Loading and Unloading Tests on Magnesium.

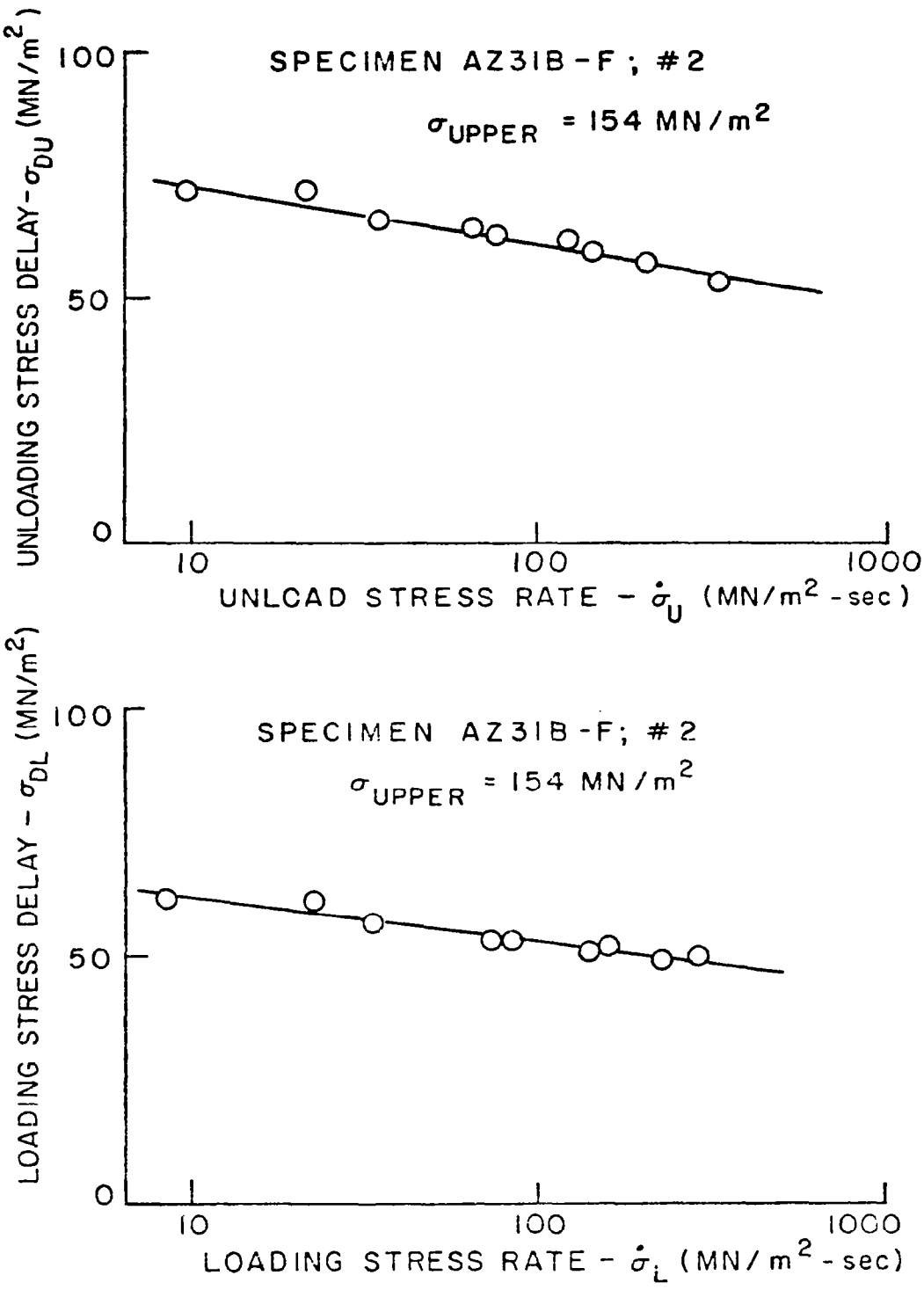

Fig. 14 Unloading and Loading Stress Delays for Various Stress Rates.